

# Highly dynamic and sensitive NEMOer calcium indicators for imaging ER calcium signals in excitable cells

Received: 7 May 2024

Accepted: 27 March 2025

Published online: 11 April 2025

 Check for updates

Wenjia Gu<sup>1,10</sup>, Jia-Hui Chen<sup>2,10</sup>, Yiyin Zhang<sup>3,10</sup>, Zhirong Wang<sup>4,10</sup>, Jia Li<sup>1,10</sup>, Sijia Wang<sup>4</sup>, Hanhan Zhang<sup>1</sup>, Amin Jiang<sup>5</sup>, Ziyi Zhong<sup>1</sup>, Jiaxuan Zhang<sup>1</sup>, Ze Xu<sup>3</sup>, Panpan Liu<sup>1</sup>, Chao Xi<sup>1</sup>, Tingting Hou<sup>3</sup>, Donald L. Gill<sup>6</sup>, Dong Li<sup>5</sup>, Yu Mu<sup>4</sup> ✉, Shi-Qiang Wang<sup>3</sup> ✉, Ai-Hui Tang<sup>7,8</sup> ✉ & Youjun Wang<sup>1,9</sup> ✉

The Endoplasmic/sarcoplasmic reticulum (ER/SR) is central to calcium (Ca<sup>2+</sup>) signaling, yet current genetically encoded Ca<sup>2+</sup> indicators (GECIs) cannot detect elementary Ca<sup>2+</sup> release events from ER/SR, particularly in muscle cells. Here, we report NEMOer, a set of organellar GECIs, to efficiently capture ER Ca<sup>2+</sup> dynamics with increased sensitivity and responsiveness. NEMOer indicators exhibit dynamic ranges an order of magnitude larger than G-CEPIA1er, enabling 2.7-fold more sensitive detection of Ca<sup>2+</sup> transients in both non-excitabile and excitable cells. The ratiometric version further allows super-resolution monitoring of local ER Ca<sup>2+</sup> homeostasis and dynamics. Notably, NEMOer-f enabled the inaugural detection of Ca<sup>2+</sup> blinks, elementary Ca<sup>2+</sup> releasing signals from the SR of cardiomyocytes, as well as in vivo spontaneous SR Ca<sup>2+</sup> releases in zebrafish. In summary, the highly dynamic NEMOer sensors expand the repertoire of organellar Ca<sup>2+</sup> sensors that allow real-time monitoring of intricate Ca<sup>2+</sup> dynamics and homeostasis in live cells with high spatiotemporal resolution.

Calcium (Ca<sup>2+</sup>) signaling is indispensable for the orchestration of multiple cellular functions and physiological processes<sup>1</sup>. As one of the major Ca<sup>2+</sup> sources and internal stores in animal cells, endoplasmic/sarcoplasmic reticulum (ER/SR) takes center stage in the choreography of calcium signaling<sup>2</sup>. Dysregulated ER homeostasis, recognized as an instigator of ER stress and apoptosis<sup>3</sup>, is associated with various diseases, including cancer, cardiovascular disorders,

and neurodegenerative diseases<sup>4,5</sup>. To better unveil the roles of ER Ca<sup>2+</sup> in health and disease, it is imperative to visualize the spatiotemporal dynamics of ER/SR Ca<sup>2+</sup> with high precision and resolution.

By introducing Ca<sup>2+</sup>-binding site into fluorescence proteins, or via mutagenesis of Ca<sup>2+</sup>-binding-domain of cytosolic GECIs like Cameleon<sup>6</sup>, GCaMP<sup>7,8</sup>, GECO<sup>9</sup>, or aequorin<sup>10</sup>, researchers have developed over a dozen sensors with relatively low Ca<sup>2+</sup> affinities (K<sub>d</sub> > 400 μM). Notable

<sup>1</sup>Beijing Key Laboratory of Gene Resource and Molecular Development, College of Life Sciences, Beijing Normal University, Beijing, China. <sup>2</sup>Department of Anatomy, School of Basic Medicine, Anhui Medical University, Hefei, Anhui, China. <sup>3</sup>State Key Laboratory of Membrane Biology, College of Life Sciences, Peking University, Beijing, China. <sup>4</sup>Institute of Neuroscience, State Key Laboratory of Neuroscience, Center for Excellence in Brain Science and Intelligence Technology, Chinese Academy of Sciences, Shanghai, China. <sup>5</sup>National Laboratory of Biomacromolecules, CAS Center for Excellence in Biomacromolecules, Institute of Biophysics, Chinese Academy of Sciences, Beijing, China. <sup>6</sup>Department of Cellular and Molecular Physiology, Pennsylvania State University College of Medicine, Hershey, PA, USA. <sup>7</sup>Anhui Province Key Laboratory of Biomedical Imaging and Intelligent Processing, Institute of Artificial Intelligence, Hefei Comprehensive National Science Center, Hefei, China. <sup>8</sup>Hefei National Research Center for Physical Sciences at the Microscale, Division of Life Sciences and Medicine, University of Science and Technology of China, Hefei, China. <sup>9</sup>Key Laboratory of Cell Proliferation and Regulation Biology, Ministry of Education, College of Life Sciences, Beijing Normal University, Beijing, China. <sup>10</sup>These authors contributed equally: Wenjia Gu, Jia-Hui Chen, Yiyin Zhang, Zhirong Wang, Jia Li. ✉e-mail: [my@ion.ac.cn](mailto:my@ion.ac.cn); [wsq@pku.edu.cn](mailto:wsq@pku.edu.cn); [tangah@ustc.edu.cn](mailto:tangah@ustc.edu.cn); [wyoujun@bnu.edu.cn](mailto:wyoujun@bnu.edu.cn)

examples of ER/SR  $\text{Ca}^{2+}$  include YC4er, CatchER sets<sup>11–13</sup>, GCaMPER<sup>14</sup>, CEPIA1er based series<sup>15–18</sup>, and erGAP2/3<sup>19</sup>. However, these ER-resident green GECIs among them often exhibit limited dynamic ranges ( $<5$ )<sup>13,15</sup> or relatively slow kinetics<sup>14</sup>, thereby impeding real-time monitoring of rapid  $\text{Ca}^{2+}$ -modulated events. To accurately capture elementary local ER  $\text{Ca}^{2+}$  changes<sup>20,21</sup>, such as  $\text{Ca}^{2+}$  blinks in cardiac muscle cells<sup>22</sup>, an ideal ER GECI should satisfy the following criteria: low  $\text{Ca}^{2+}$  affinity, large dynamics, and rapid kinetics.

Mostly by mutating  $\text{Ca}^{2+}$ -binding residues in our recently developed NEMO indicators<sup>23</sup>, we present herein a set of highly dynamic and sensitive green GECIs tailored for ER/SR, termed NEMOer, along with its ratiometric version TuNer. Basal fluorescence and responses of NEMOer indicators can be one order of magnitude larger than G-CEPIA1er, reporting significantly larger  $\text{Ca}^{2+}$  oscillation signals. TuNer sensors enable super-resolution recording of SR/ER  $\text{Ca}^{2+}$  homeostasis and dynamics. With the NEMOer-f variant, we successfully detect  $\text{Ca}^{2+}$  blink, the elementary  $\text{Ca}^{2+}$  releasing signal from SR of cardiomyocytes, as well as in vivo spontaneous SR  $\text{Ca}^{2+}$  releasing event in zebrafish. Collectively, the highly dynamic NEMOer sensors hold high potential for a wide range of applications in monitoring ER  $\text{Ca}^{2+}$  dynamics and homeostasis within live cells.

## Results

### Engineering of low $\text{Ca}^{2+}$ affinity NEMOer indicators

By introducing known  $\text{Ca}^{2+}$ -affinity-reducing mutations into the calmodulin domain of NEMO indicators<sup>15,23</sup> and adding ER-targeting sequences, we generated NEMO variants for monitoring ER  $\text{Ca}^{2+}$ , and screened their performance in HEK293 cells (Fig. 1A–C, and Supplementary Tables 1–2). Basic sensor properties, including their basal fluorescence ( $F_0$ ), maximal ( $F_{\text{max}}$ ), and minimal ( $F_{\text{min}}$ ) fluorescence were obtained in cells transiently expressing these variants at comparable levels. Two well-known ER  $\text{Ca}^{2+}$  sensors G-CEPIA1er<sup>15</sup> and ER-GCaMP6-150<sup>24</sup> were used as controls. Briefly, after the recording of  $F_0$ ,  $F_{\text{min}}$  was measured by depleting ER  $\text{Ca}^{2+}$  store with 2.5  $\mu\text{M}$  ionomycin (iono; a  $\text{Ca}^{2+}$  ionophore) and subsequent permeabilization using 25  $\mu\text{M}$  digitonin. In the end, large amount of  $\text{Ca}^{2+}$  (30 mM) was added to the bath containing 25  $\mu\text{M}$  digitonin to induce  $F_{\text{max}}$  in permeabilized cells (Fig. 1B). Fluorescence responses relative to  $F_{\text{min}}$  (Fig. 1C), mean  $F_0$  and dynamic range (DR) values defined as  $\Delta F/F_{\text{min}}$ , or  $(F_{\text{max}} - F_{\text{min}})/F_{\text{min}}$  (Fig. 1D) were plotted to visualize the full capacity of these low  $\text{Ca}^{2+}$  affinity NEMOer variants.

Five best-performing constructs with bright  $F_0$  and large DR values (Fig. 1D) were selected and named as mNeonGreen-based Calcium indicator for ER (NEMOer). These include the medium (NEMOer-m) for general use, high contrast (NEMOer-c) for high contrast applications, fast (NEMOer-f) for rapid signal detection, bright (NEMOer-b) for low-phototoxicity scenarios, and sensitive (NEMOer-s) for detecting subtle fluctuations in ER  $\text{Ca}^{2+}$  levels.

We next determined performance of NEMOer variants both in vitro and in situ. The affinities of NEMOer variants were reduced to near millimolar (mM) ranges (Supplementary Fig. 1A; Fig. 1E), either comparable to that of G-CEPIA1er (706  $\pm$  48  $\mu\text{M}$  in situ) or significantly lower. And the  $\text{Ca}^{2+}$  dissociation kinetics of NEMOer-f ( $k_{\text{off}} = 156.75 \pm 3.11 \text{ s}^{-1}$ ) is comparable to that of G-CEPIA1er (131.47  $\pm$  7.07  $\text{ s}^{-1}$ , Supplementary Fig. 1B), whereas the  $k_{\text{off}}$  values of other NEMOer sensors are markedly slower (ranging from approximately 17–36  $\text{ s}^{-1}$ ). This highlights NEMOer-f as particularly well-suited for decoding fast acting ER  $\text{Ca}^{2+}$  signals in excitable cells, whereas the slower NEMOer variants are restricted to detecting changes occurring with time constants under 60 ms.

More careful in situ characterization revealed that the in cellulo DR of NEMOer sensors are superior to other ER GECIs tested side-by-side. In HEK293 cells, ER-GCaMP6-150 showed a  $F_0$  that was close to its  $F_{\text{max}}$ , indicating that it is close to saturation at the basal condition (Fig. 1B, C). We thus only used G-CEPIA1er as a reference as it showed a

good combination of affinity, kinetics and DR<sup>15</sup> (Fig. 1B, C). In HeLa cells, the DR values of NEMOer-f and NEMOer-b, 68.3 and 139.3, respectively, were 14.3 to 29.9-fold higher than that of G-CEPIA1er (4.5). The DRs of NEMOer-m, NEMOer-s and NEMOer-c were further increased (263.3, 253.8, or 349.3, respectively) to be over 50-fold higher than that of G-CEPIA1er (Fig. 1E). Overall, NEMOer indicators represent a class of bright ER  $\text{Ca}^{2+}$  indicators with the in cellulo DRs up to 80-fold larger than G-CEPIA1er.

All NEMOer variants showed in vitro DR values larger than 120-fold (Supplementary Fig. 1A, left), at least 18.8 fold larger than that of G-CEPIA1er (6.4  $\pm$  0.1). Similar to their corresponding template<sup>23</sup>, the cause of these significantly large DR values is a greater  $\text{Ca}^{2+}$ -dependent fold-of-increase in the molecular brightness of the anionic fluorophores in NEMOer variants (Supplementary Fig. 1C–G; Supplementary Table 3). In the absence of  $\text{Ca}^{2+}$ , the anionic fluorophore of NEMOer-c (0.16  $\pm$  0.03  $\text{ mM}^{-1}\text{ cm}^{-1}$ ) is considerably dimmer, approximately one-fourth that of G-CEPIA1er. And the brightness of  $\text{Ca}^{2+}$ -saturated anionic NEMOer-c (54.85  $\pm$  2.19  $\text{ mM}^{-1}\text{ cm}^{-1}$ ), more than ten times that of G-CEPIA1er.

Consistent with the observation that the basal fluorescence ( $F_0$ ) of NEMOer sensors were much brighter than that of G-CEPIA1er (Fig. 1D), over 87% of G-CEPIA1er fluorophores exist in neutral state, the relative dim and less  $\text{Ca}^{2+}$ -sensitive configuration, while up to 75% of the fluorophore within NEMOer-c could exist in its bright anionic form (Supplementary Table 3). We next more carefully compared  $F_0$  of NEMOer indicators with G-CEPIA1er using a P2A-based bicistronic vector to drive the co-expression of GECIs and mKate as an expression marker at a near 1:1 ratio. The normalized basal GECI brightness was shown as the fluorescence ratio of GECI over mKate (Fig. 1F). As expected, all NEMOer sensors showed significantly higher basal brightness than that of G-CEPIA1er, with NEMOer-f the dimmest and NEMOer-b the brightest among all NEMOer variants. Even when examined with settings optimized for G-CEPIA1er (GFP filters),  $F_0$  of NEMOer-f and NEMOer-b was about 3 or 8.5 fold of G-CEPIA1er, respectively. When a filter set (YFP) optimized for NEMOer was used, NEMOer-f and NEMOer-b were 7.4 and 17.4 folds brighter than G-CEPIA1er.

NEMOer indicators also showed significantly enhanced photostability than G-CEPIA1er (Supplementary Fig. 2A, B). NEMOer-f exhibited remarkable photostability, enduring illumination over 50 times stronger (0.57 mW) than that applied to G-CEPIA1er (0.01 mW) without apparent photobleaching. The increase in light intensity (from 0.01 mW to 0.57 mW) led to more than a 10-fold rise in the basal fluorescence of NEMOer-f (Supplementary Fig. 2), making it highly suitable for imaging scenarios requiring intense excitation, such as monitoring  $\text{Ca}^{2+}$  signals with super-resolution imaging system, or in vivo imaging of subcellular compartments such as dendrites.

Together, these results firmly establish NEMOer indicators as a class of highly bright, photostable GECIs with extraordinarily large  $\text{Ca}^{2+}$ -dependent changes in fluorescence.

### Performance of NEMOer indicators in non-excitabile cells

We first examined the ability of NEMOer indicators to report the depletion of ER  $\text{Ca}^{2+}$  stores induced by various stimuli. Consistent with their large DR values, in responses to full ER store depletion triggered by ionomycin, NEMOer indicators showed more than 95.8% decreases in fluorescence, significantly larger than those from G-CEPIA1er (71.9  $\pm$  1.3%) (Fig. 2A). In response to sub-maximal activation of muscarinic acetylcholinergic receptors with carbachol (CCh, 10  $\mu\text{M}$ ), NEMOer indicators showed stronger response with the mean peak amplitudes 2.1–2.4 folds higher than G-CEPIA1er (Fig. 2B). Both NEMOer-f and G-CEPIA1er recover to a plateau lower than baseline, with the NEMOer-f signal reaching a smaller plateau (0.65  $\pm$  0.14 vs. 0.93  $\pm$  0.06, respectively) and recovering at a slower rate (half-rise time: 4.47  $\pm$  0.11 vs. 3.51  $\pm$  0.20). Given that G-CEPIA1er and NEMOer-f

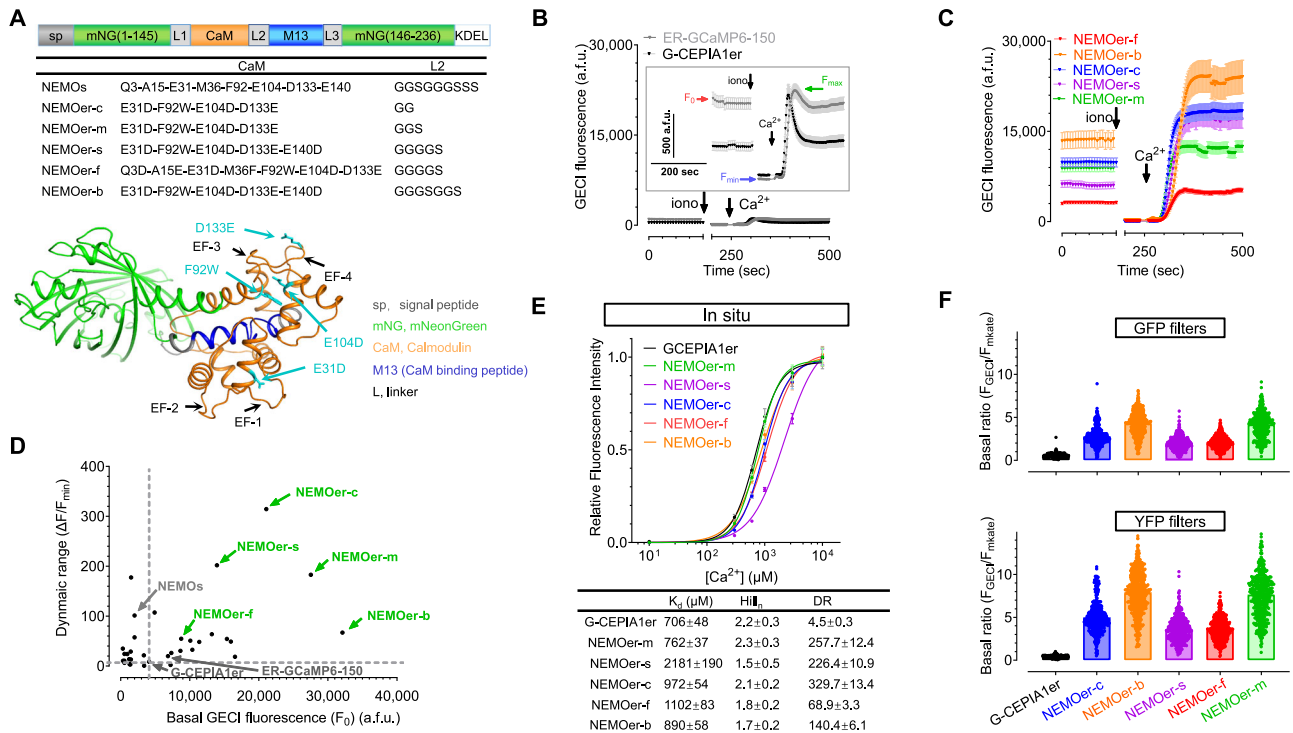


**Fig. 1 | Screening and ex vivo characterization of NEMOer indicators.** **A** NEMOer sensors are generated by introducing amino acid substitutions in calmodulin region of NEMO indicators. Top, a diagram showing the design of NEMOer variants. Middle, key amino acids substitutions. Bottom, predicted NEMOer-s structure by I-TASSER<sup>41</sup> (Iterative Threading ASSEMBly Refinement). Four loops of EF-hands (EF) within calmodulin domain of NEMOer sensors are indicated by black arrows. **B–E** Screening of NEMOer variants in non-excitable mammalian cells.  $Ca^{2+}$ -imaging-based screening assay shown by typical traces from ER-GCaMP6-150, G-CEPIA1er (**B**) or NEMOer variants (**C**) -expressing cells. Inserts, traces with enlarged scales. After recording the basal fluorescence ( $F_0$ ), endoplasmic reticulum  $Ca^{2+}$  store was depleted with 2.5  $\mu M$  ionomycin (iono) to obtain minimal GECl fluorescence ( $F_{min}$ ). Cells were permeabilized with 30 mM  $Ca^{2+}$  imaging solution containing 25  $\mu M$  digitonin to obtain maximal response ( $F_{max}$ ). The observed peak-followed-by-a-decay-to-plateau phenomenon for G-CEPIA1er and ER-GCaMP6-150, likely due to

the harsh imaging protocol, remains to be elucidated. (For typical trace in **(B, C)**, G-CEPIA1er,  $n = 33$  cells; ER-GCaMP6-150,  $n = 40$  cells; NEMOer-m,  $n = 30$  cells; NEMOer-s,  $n = 36$  cells; NEMOer-f,  $n = 38$  cells; NEMOer-c,  $n = 35$  cells; NEMOer-b,  $n = 27$  cell). **D** Scatter plot of  $F_0$ -mean dynamic range (DR;  $(F_{max} - F_{min})/F_{min}$ ) of the indicated GECl. **E** In situ dose-response curves of NEMOer sensors. Top, typical traces; Bottom, statistics (G-CEPIA1er,  $n = 52$  cells; NEMOer-m,  $n = 56$  cells; NEMOer-s,  $n = 63$  cells; NEMOer-f,  $n = 46$  cells; NEMOer-c,  $n = 57$  cells; NEMOer-b,  $n = 52$  cell). **F** Basal brightness of NEMOer or G-CEPIA1er viewed with YFP (top) or GFP (bottom) filters. To estimate the basal fluorescence of GECl ( $F_{GECI}$ ), cells expressing mKate-P2A-GECl were normalized against the fluorescence of mKate, an expression marker ( $F_{mKate}$ ). (G-CEPIA1er,  $n = 390$  cells; NEMOer-m,  $n = 431$  cells; NEMOer-s,  $n = 421$  cells; NEMOer-f,  $n = 469$  cells; NEMOer-c,  $n = 411$  cells; NEMOer-b,  $n = 473$  cell). **B, C, E, F** Data shown as mean  $\pm$  s.e.m. **B–F** Three independent biological replicates,  $\geq 17$  cells per repeat.

are kinetically similar (Supplementary Fig. 1B, Supplementary Table 2) and that NEMOer-f is more sensitive, these results suggest that, after the initial  $Ca^{2+}$  release induced by CCh, the subsequent ER  $Ca^{2+}$  refilling occurs more slowly and less efficiently than previously estimated. Similarly, NEMOer sensors also showed superior performance in reporting  $Ca^{2+}$  oscillations over G-CEPIA1er (Fig. 2C). Notably, while the time courses of  $Ca^{2+}$  oscillations detected by NEMOer variants are similar (Fig. 2C), the time-to-nadir of the first CCh-induced transient decay for the other NEMOer variants occur approximately 3–5 s later than those measured by G-CEPIA1er and NEMOer-f. This suggests that the slower NEMOer variants may be less effective at accurately capturing rapid ER  $Ca^{2+}$  decays (Fig. 2B). Consistent with the observed superior performance in NEMOer sensors, simulation results based on the Hill equation and in situ parameters demonstrate that GECl with larger DRs indeed exhibit significantly enhanced responses (Fig. 2D).

To better assess whether the fast NEMOer-f sensors could reliably follow cytosolic  $Ca^{2+}$  oscillations with bigger responses, we co-expressed a cytosolic red GECl, R-GECO1.2<sup>25</sup>, with either NEMOer-f or G-CEPIA1er in HEK293 cells. 10  $\mu M$  CCh induced synchronized changes in R-GECO1.2 and G-CEPIA1er or NEMOer-f fluorescence (Fig. 2E, top left panel). Notably, while G-CEPIA1er only detected synchronized ER  $Ca^{2+}$  oscillations in 50% cells with cytosolic  $Ca^{2+}$  oscillations as indicated by R-GECO1.2 signal, NEMOer-f successfully captured all events,

establishing it as a more reliable indicator for monitoring ER  $Ca^{2+}$  oscillations (Fig. 2E, top right panel). The cytosolic  $Ca^{2+}$  increases observed with R-GECO1.2 were comparable between the two groups (Fig. 2E, bottom left two panels), indicating a similar reduction in ER  $Ca^{2+}$  levels. However, in response to the first ER  $Ca^{2+}$  release, NEMOer-f exhibited 2.7-fold larger responses compared to G-CEPIA1er (Fig. 2E, bottom right panel). This superior sensitivity of NEMOer-f in reporting sub-maximal ER  $Ca^{2+}$  releases is likely due to its higher  $K_d$  and DR values. These results establish that NEMOer-f indicator is more sensitive than G-CEPIA1er, and exhibits the necessary speed to capture ER  $Ca^{2+}$ -releasing events that drive cytosolic  $Ca^{2+}$  oscillations. Together, intensimetric NEMOer response to these investigated  $Ca^{2+}$  signals in non-excitable cells are remarkably larger than those of G-CEPIA1er tested side-by-side.

To enable monitoring of ER  $Ca^{2+}$  homeostasis, we generated ratiometric mTurquoise2- NEMOer (TuNer) indicators by using a mTurquoise2 (mTq2) variant as both an indicator for the sensor expression level and a Förster energy resonance transfer (FRET) donor for NEMOer sensors (Supplementary Fig. 3A). We reasoned that the FRET efficacy between mTq2 and NEMOer indicators may be proportional to NEMOer fluorescence. This would ensure reciprocal change in NEMOer and mTq2 fluorescence, resulting in amplified NEMOer responses (Supplementary Fig. 3B). Since ER  $Ca^{2+}$  level is less

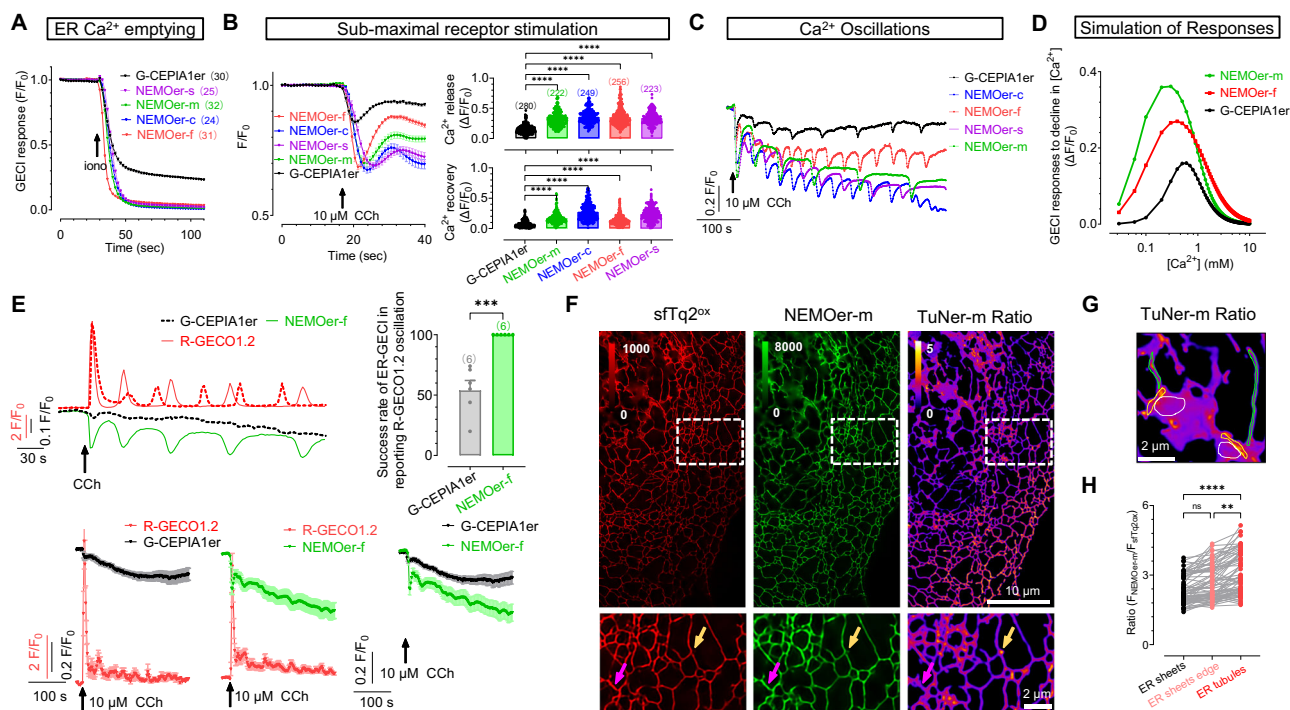


**Fig. 2 | Performance of NEMOer sensors in non-excitable mammalian cells.**

**A** Typical ER- $\text{Ca}^{2+}$  responses in HEK293 cells induced by ionomycin (iono, 2.5  $\mu\text{M}$ ). **B**, **C** G-CEPIA1er or NEMOer responses to ER- $\text{Ca}^{2+}$ -lowering by submaximal receptor stimulation with carbachol (CCh, 10  $\mu\text{M}$ ) in HEK293 cells. Initial ER  $\text{Ca}^{2+}$  decreasing recorded in nominally  $\text{Ca}^{2+}$  free solution. Left, typical traces; right, statistics.

**B** ( $****P < 1E-15$ , one-way ANOVA). **C** Typical cells showing ER  $\text{Ca}^{2+}$  oscillations in 2 mM  $\text{Ca}^{2+}$  imaging solution. **D** Simulated  $F/F_0$  vs.  $[\text{Ca}^{2+}]_{\text{ER}}$ , assuming a 20%  $[\text{Ca}^{2+}]_{\text{ER}}$  drop due to ER  $\text{Ca}^{2+}$  release. The simulation was performed using the Hill equation and in situ parameters from Fig. 1E, with  $F_{\text{min}}$  set to 1. **E** Simultaneous monitoring of 10  $\mu\text{M}$  CCh-induced  $\text{Ca}^{2+}$  oscillations in ER and cytosol in HEK293 cells. NEMOer-f or G-CEPIA1er was transiently co-expressed with the cytosolic red indicator, R-GECO1.2. Top left, representative response traces; top right, statistics. ( $***P = 0.0002$ , unpaired Student's *t*-test, two-tailed.) Bottom, averaged response traces of R-GECO1.2 together with corresponding G-CEPIA1er or NEMOer-f (left two

panels), and a direct comparison of the responses between NEMOer-f and G-CEPIA1er (right panel). **F–H** Ratiometric signals of mTurquoise2-NEMOer-m (TuNer-m) in COS-7 cells collected with multimodality structured illumination microscopy (Multi-SIM). The TuNer ratio (*R*) is defined as  $R = F_{\text{NEMOer}}/F_{\text{sTtq2ox}}$ . **(F)** Typical basal fluorescence and ratiometric images, with enlarged views. Purple arrows show higher fluorescence with a lower ratio, and yellow arrows indicate the opposite. TuNer-m ratios within ER sheets and tubules. **(G)** Diagram of Region of Interest (ROI) selection in ratio image: ER sheets (white circles), ER sheets edge (yellow circles) or ER tubules (green circles) **(H)** Statistics of **(F)**, mean size: sheets  $0.06 \pm 0.01 \mu\text{m}^2$ , edge  $0.07 \pm 0.01 \mu\text{m}^2$ , tubules  $0.07 \pm 0.01 \mu\text{m}^2$ . ( $****P = 1E-7$ ,  $**P = 0.0019$ ,  $ns P = 0.0723$ , one-way ANOVA,  $n = 70$  ROIs from at least 15 cells). 3 independent biological replicates,  $\geq 5$  cells per repeat. **A–C** 3 independent biological replicates,  $\geq 15$  cells per repeat. **(A, B, C, E)** Error bar denotes SEM.

conveniently manipulatable as compared with cytosolic  $\text{Ca}^{2+}$ , we used cytosolic mNeonGreen based indicator NCaMP7<sup>26</sup> to optimize the linkers and interfaces between the FRET pair (Supplementary Table 4), and then applied the optimized strategy for NEMO and NEMOer sensors to obtain ratiometric mTurquoise2-NEMO (TurN, cytosolic version) or TuNer sensors (Supplementary Table 5, 6). The DRs of all these TurN indicators were 1.4–2 fold higher than the corresponding monofluorescent templates (Supplementary Tables 4–6). When stimulated with 10  $\mu\text{M}$  CCh, decreases in ratios of TuNer indicators were more than 1.5-fold of miGer, a ratiometric ER  $\text{Ca}^{2+}$  indicator based on G-CEPIA1er (Supplementary Fig. 3C). This finding aligns with the data from monomeric indicators (-1.7-fold, Fig. 2B–D). When measured with TuNer sensors, the basal ER  $\text{Ca}^{2+}$  levels within HEK293 and HeLa cells fell in the range of 0.8–1.3 mM (Supplementary Fig. 3D).

We further examined TuNer-m responses with a commercial confocal imaging system, coupled with offline sparse deconvolution analysis<sup>27</sup>, to obtain super resolution time-lapsed images. Tubular ER structure within COS-7 cells transiently expressing TuNer-m was clearly visible with a good signal-to-noise ratio (Supplementary Fig. 4A, B). Nuclear  $\text{Ca}^{2+}$  signaling is crucial for proper cell function<sup>28</sup>, yet nuclear ER  $\text{Ca}^{2+}$  content has been less studied. Here we observed that basal nuclear ER  $\text{Ca}^{2+}$  levels are slightly, but significantly higher than the rest portion of ER (indicated by white and yellow circles, respectively, Supplementary Fig. 4A, C). Further analysis showed that the TuNer-m ratio also differed significantly among different

subcellular areas at rest, demonstrating uneven distribution of resting ER  $\text{Ca}^{2+}$  levels (Supplementary Fig. 4D). When examined with structured illumination microscopy (SIM) super-resolution imaging, the TuNer-m ratios within ER tubules are higher than the adjacent ER sheets in COS-7 cells (Fig. 2F–H), suggesting that  $\text{Ca}^{2+}$  levels within ER sheets are significantly lower than those in their corresponding neighboring ER tubules.

Of note, the basal subcellular NEMOer-m fluorescence does not correlate with that of TuNer-m ratio (microdomains indicated by arrows, Fig. 2F and Supplementary Fig. 4B), clearly demonstrating an uneven distribution of GECIs within ER. The mean peak basal  $\text{Ca}^{2+}$  concentration in the hot spots are approximately 1.9–2.0 mM, about two-folds higher than in adjacent  $\text{Ca}^{2+}$  microdomain (~0.9 mM) (Fig. 2F). Upon stimulation with 5  $\mu\text{M}$  ATP, different subcellular regions of COS-7 cells showed repetitive fluctuations of TuNer-m ratios with varying amplitudes, illustrating slightly unsynchronized  $\text{Ca}^{2+}$  oscillations (Supplementary Fig. 4E, Supplementary Video 1). The discrepancies between NEMOer-m signals and TuNer-m ratios within microdomains are more pronounced in enlarged pictures or zoom-in videos (Dots indicated by white arrows, Supplementary Fig. 4B and Supplementary Video 2). These results thus underscore the need for caution when interpreting results obtained with intensimetric GECIs.

During ER  $\text{Ca}^{2+}$  oscillations induced by 5  $\mu\text{M}$  ATP (Supplementary Fig. 4E) as well as dynamic re-arrangements of ER tubules, we could clearly see transient punctate microdomains with higher TuNer-m

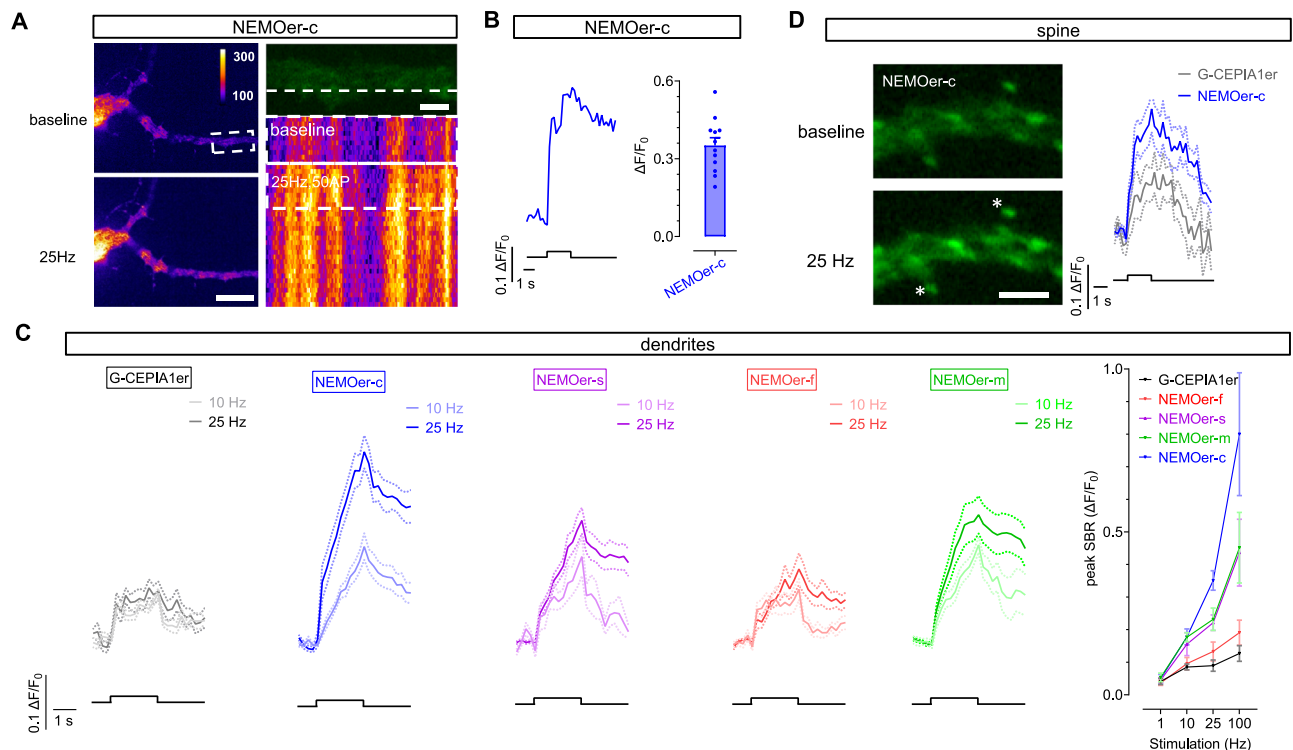


**Fig. 3 | Responses of NEMOer variants or G-CEPIA1er to electric field stimulation in rat hippocampal neurons.** **A** Typical images showing the fluorescence distribution and responses of NEMOer-c to 25 Hz field stimulation. Pseudocolor cellular images of NEMOer-c before (top left) and after 50 AP (25 Hz) stimulation (bottom left) (scale bar, 10  $\mu$ m). Enlarged view of the dendrite region (top right), with a white dashed line indicating the position of line scan. Kymograph showing NEMOer-c responses to 25 Hz stimulation within a dendritic region (bottom right) along the indicated line. Scale bar, 2  $\mu$ m. **B** Representative tracing of NEMOer-c responses to 25 Hz stimulation, right, statistics ( $n = 12$  cells). Error bar denotes SEM.

**C** Response of NEMOer variants or G-CEPIA1er within dendrites induced by electric stimulation with varies frequencies, with mean response curves shown on the left and statistics shown on the rightmost. Error bars denote SEM. (For stimulation at varied frequencies, G-CEPIA1er,  $n = 11, 11, 12, 14$  cells; NEMOer-f,  $n = 15, 14, 12, 13$  cells; NEMOer-s,  $n = 11, 13, 12, 13$  cells; NEMOer-m,  $n = 14, 17, 16, 13$  cells; NEMOer-c,  $n = 13, 14, 12, 12$  cells). **D** Typical images showing the individual spine fluorescence and responses of NEMOer-c to 25 Hz field stimulation. Scale bar, 2  $\mu$ m. Right, statistics. Error bars denote SEM. (G-CEPIA1er,  $n = 36$  spines; NEMOer-c,  $n = 68$  spines).

ratios (Dots indicated by white arrows, Supplementary Video 3), highlighting the highly discrete nature of  $\text{Ca}^{2+}$  refilling within ER tubules. Transient “Moving dark dots” with decreased TuNer-m ratios were also observed (pointed by yellow arrows, Supplementary Video 3), likely representing the brief reductions of ER  $\text{Ca}^{2+}$  levels within microdomains of ER tubules that are responsible for propagating cytosolic  $\text{Ca}^{2+}$  waves. To the best of our knowledge, this is the first report to visualize organelle dynamics and concurrent ER  $\text{Ca}^{2+}$  signals in microdomains with super-resolution.

Collectively, our mostly proof-of-concept data show that the bright and sensitive TuNer sensors are well suited for super-resolution imaging of dynamic ER  $\text{Ca}^{2+}$  signaling in non-excitable cells.

### Performance of NEMOer sensors in cultured neurons

We proceeded to investigate NEMOer responses in cultured primary hippocampal neurons under electrical field stimulation. Since it is established that excited neurons often show ER  $\text{Ca}^{2+}$  overload<sup>14,24,29</sup>, we expressed NEMOer-c variant in cultured primary hippocampal neurons, and examined its ability to report ER  $\text{Ca}^{2+}$  signals induced by electrical field stimulation. In transiently transfected neurons, NEMOer-c fluorescence displayed an ER-like reticular network resembling the endoplasmic reticulum in both dendrites and soma. With a train of 50 action potentials (APs) at 25 Hz stimulation, we observed a robust increase in NEMOer-c fluorescence, with dendrites showing a more pronounced response compared to the soma (Fig. 3A, B), indicating more ER  $\text{Ca}^{2+}$  overload in dendrites. Next, we examined the responses of other NEMOer variants following stimulations of 10 Hz,

25 Hz or higher frequency, and found that NEMOer sensors had a dramatic increase in the peak signal-to-background ratio (SBR) compared to the G-CEPIA1er sensor. Notably, the NEMOer-c sensors had the highest response amplitude, while NEMOer-c and NEMOer-f were fast enough to pick up individual responses to 10 Hz stimulation (Fig. 3C).

Subsequently, we detected spines  $\text{Ca}^{2+}$  signals elicited by 50 AP at 25 Hz in secondary dendrites of hippocampal neurons. Compared to signals in G-CEPIA1er-expressing neurons, the 50AP-induced spines transient  $\text{Ca}^{2+}$  response in NEMOer-c-expressing neurons was significantly enhanced (Fig. 3D), while the other NEMOer variants showed a similar response. These results suggest that NEMOer sensors are capable of effectively responding to synaptic ER  $\text{Ca}^{2+}$  dynamics in primary hippocampal neurons.

To further verify if the responses reported by NEMOer sensors represent  $\text{Ca}^{2+}$  increase in ER, we examined the effects of SERCA inhibition by incubating cells with cyclopiazonic acid (CPA) for one hour and then stimulating them at a frequency of 100 Hz for 2 s. As expected, the NEMOer-c and NEMOer-s signals were significantly reduced in response to the stimulation in the presence of CPA compared to DMSO (0.33 vs 0.81 (peak response in CPA vs DMSO),  $P = 0.02$ ; 0.12 vs 0.46 (peak response in CPA vs DMSO),  $P = 0.004$ , respectively). These results suggest that NEMOer sensors have a significantly superior ER  $\text{Ca}^{2+}$  responses to physiological frequency stimulations in primary neurons compared to G-CEPIA1er sensors.

We also assessed GECIs' responses to ER  $\text{Ca}^{2+}$  lowering induced by 100  $\mu$ M 3,4-Dihydroxyphenylglycol (DHPG), which activates

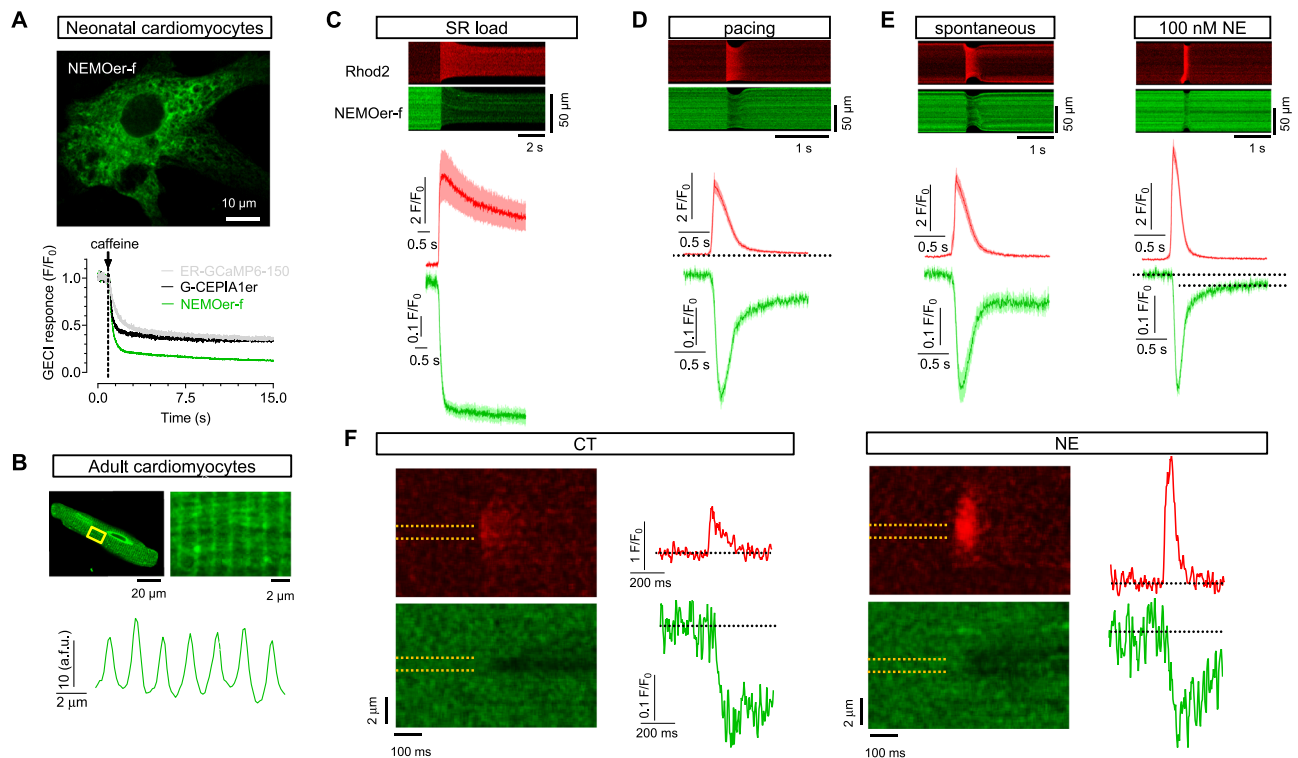


**Fig. 4 | Performances of NEMOer sensors in monitoring sarcoplasmic reticulum (SR)  $\text{Ca}^{2+}$  dynamics in cardiomyocytes.** **A** SR load measurement by 30 mM caffeine perfusion in neonatal rat cardiomyocytes. Top, pseudocolor image showing a typical cell expressing NEMOer-f; bottom, averaged time curves showing caffeine-induced responses of transiently expressed indicators. The arrow indicates the time of caffeine stimulation. Scale bar, 10  $\mu\text{m}$ . Typical figure captured from 6 cells across 75 one-day-old Sprague-Dawley rats in three independent experiments, showing consistent reproducibility across experiments. **B** Subcellular distribution of NEMOer-f fluorescence in adult rat cardiomyocyte revealed with confocal imaging. Top left, typical confocal images; top right, enlarged view of boxed area shown in top left image; bottom trace, spatial profile for the boxed region. Typical figure captured from 15 cells across 3 adult rats in three independent experiments, showing consistent reproducibility across experiments. **C–E** Local and global

cytosolic and SR  $\text{Ca}^{2+}$  dynamics in adult rat cardiac myocytes revealed by dual-color imaging using NEMOer-f and a cytosolic  $\text{Ca}^{2+}$  indicator, Rhod-2. Top, typical line-scan images; bottom, corresponding mean time course plots.  $\text{Ca}^{2+}$  responses induced by caffeine (30 mM) (**C**). Local SR  $\text{Ca}^{2+}$  scraps and accompanying cytosolic  $\text{Ca}^{2+}$  transients are triggered by electric field stimulation (**D**) or during a spontaneous release (**E**), either under control (CT) (left) or when treated with 100 nM norepinephrine (NE) (right). (**C**,  $n = 6$  cells; **D**,  $n = 14$  cells; **E** left trace,  $n = 11$  cells; (**E** right trace,  $n = 20$  cells. Data from 3 adult rats). Data is shown as mean  $\pm$  s.e.m. **F** Spontaneous elementary cytosolic  $\text{Ca}^{2+}$  spark and SR  $\text{Ca}^{2+}$  blink events under CT (left) or NE-treated (right) conditions revealed by Rhod-2 and NEMOer-f, respectively. Typical line-scan images are shown on the left; corresponding time-course curves are shown on the right.

metabotropic glutamate receptor (mGluR), leading to the generation of  $\text{IP}_3$  and  $\text{Ca}^{2+}$  releases from ER. In the spines of cultured rat cortical neurons, all NEMOer sensors exhibited significantly larger declines compared to G-CEPIA1er (Supplementary Fig. 5A). The amplitudes of lowering in GECI signals were comparable to those observed in HEK293 cells (Fig. 2A).

#### Performance of NEMOer sensors in cultured cardiac muscle cells

We moved on to further compare the responses of the fast-acting NEMOer-f with G-CEPIA1er in neonatal cardiomyocytes challenged with 30 mM caffeine, an agonist of ryanodine receptors (RyR), the primary  $\text{Ca}^{2+}$  releasing channels on SR. Decreases in NEMOer signals were more than 80%, significantly larger than those of G-CEPIA1er or ER-GCaMP6-150 (~66%) (Fig. 4A, Supplementary Fig. 5B–D). Specifically, NEMOer-f demonstrated the fastest kinetics among NEMOer variants, significantly faster than ER-GCaMP6-150 (decay rate constant:  $2.47 \pm 0.06 \text{ s}^{-1}$  vs  $0.81 \pm 0.02 \text{ s}^{-1}$ ,  $P = 2.37\text{E-}6$ ), indicating its capability to detect rapid SR  $\text{Ca}^{2+}$  dynamics in cardiac muscle cells.

We then infected adult rat cardiomyocytes with adenovirus carrying NEMOer-f and imaged them with confocal microscopy 36–48 h later. We found that NEMOer-f fluorescence exhibited a striated sarcomeric pattern, indicating its correct localization in the SR (Fig. 4B). To better assess NEMOer-f performance, we co-loaded cardiomyocytes with a cytosolic chemical  $\text{Ca}^{2+}$  indicator Rhod-2, and

simultaneously monitored the responses of both indicators. In response to 30 mM caffeine, Rhod-2 signal increased approximately four-fold, indicating a substantial drop in SR  $\text{Ca}^{2+}$  levels. Concurrently, NEMOer-f fluorescence rapidly decreased to about 75% of baseline, significantly surpassing values reported with a chemical indicator Fluo-5N (66.7%)<sup>30</sup>. This result highlights the high sensitivity of NEMOer-f for directly monitoring SR  $\text{Ca}^{2+}$  decreases in intact cardiomyocytes (Fig. 4C).

Next, we examined  $\text{Ca}^{2+}$  dynamics during excitation-contraction (E-C) coupling with NEMOer-f and Rhod-2. In response to field electrical stimulation (15 V, 1 Hz), cytosolic  $\text{Ca}^{2+}$  pulse indicated by Rhod-2 signal ( $\Delta F/F_0 = 3.1 \pm 0.3$ ) was accompanied by a large transient decrease in NEMOer-f fluorescence ( $\Delta F/F_0 = 0.35 \pm 0.02$ ) (Fig. 4D, Supplementary Fig. 6A), demonstrating simultaneous lowering of local SR  $\text{Ca}^{2+}$  levels, or  $\text{Ca}^{2+}$  scraps. Compared with those reported by a commercial  $\text{Ca}^{2+}$  dye (Fluo5N,  $\Delta F/F_0 = 0.1 - 0.2$ ) or R-CEPIA1er<sup>31,32</sup>,  $\text{Ca}^{2+}$  scraps indicated by NEMOer-f demonstrated a similar time-to-nadir ( $126.8 \pm 11.4 \text{ ms}$ ) and recovery time ( $414.8 \pm 26.9 \text{ ms}$ ). Nevertheless, peak NEMOer-f responses were larger than R-CEPIA1er or Fluo-5N, showcasing its increased sensitivity over these two sensors.

Using Rhod-2 and NEMOer-f, we subsequently examined the corresponding spontaneous cytosolic and SR  $\text{Ca}^{2+}$  activities under resting conditions or upon adrenergic receptor activation (100 nM norepinephrine, NE). We found that both Rhod-2 and NEMOer-f

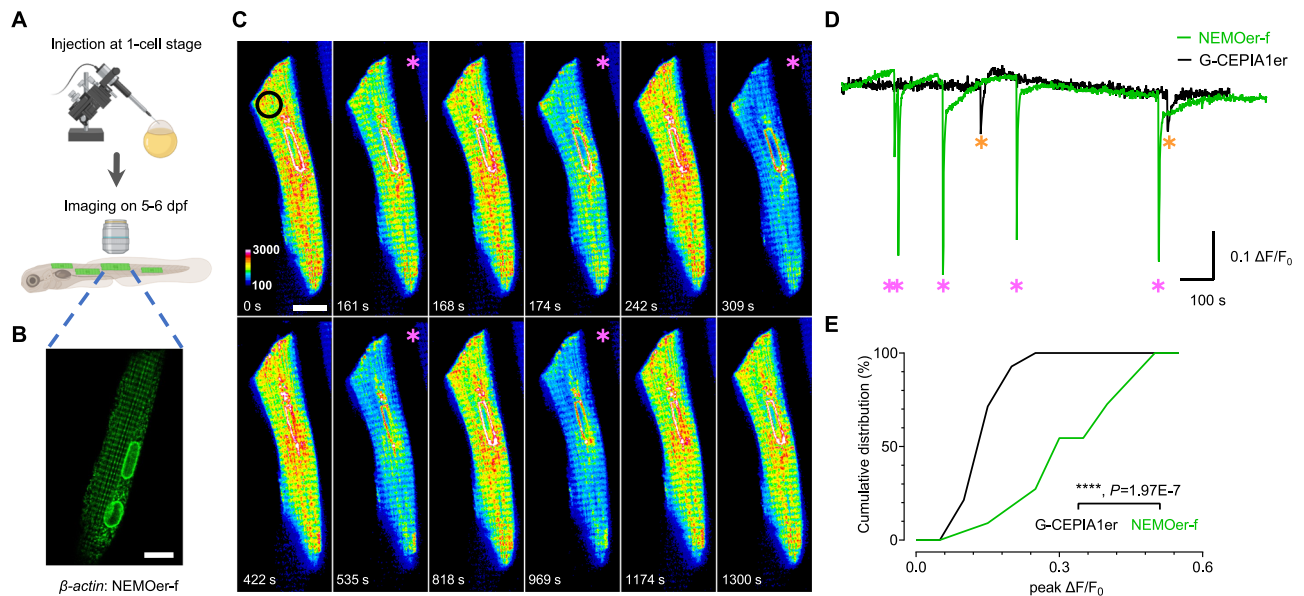


**Fig. 5 | In vivo NEMOer-f responses to spontaneous SR Ca<sup>2+</sup> releasing events in skeletal muscles of zebrafish.** **A** A schematic depiction of the NEMOer-f in vivo imaging workflow in zebrafish. Created in BioRender. Wang, Z. (2025) <https://BioRender.com/k83b811>. **B** A typical sparsely labeled skeletal muscle cell, expressing NEMOer-f. Scale bar, 10  $\mu$ m. Typical figure captured from 12 cells and 4 zebrafish larvae, showing consistent reproducibility across experiments. **C** Image montage of time-lapse imaging at 1 Hz. Black circle indicates the ROI for extracting

time series in **(D)**. Pink asterisks indicate single Ca<sup>2+</sup> events. Scale bar, 10  $\mu$ m. **D** Representative time series showing spontaneous SR Ca<sup>2+</sup> release indicated by NEMOer-f and G-CEPIA1er signal. Pink and orange asterisks indicate single NEMOer-f and G-CEPIA1er Ca<sup>2+</sup> events. **E** Cumulative distribution of amplitude of NEMOer-f responses (for NEMOer-f,  $n = 22$  events from 12 cells and 4 zebrafish larvae; for G-CEPIA1er,  $n = 14$  events from 9 cells and 4 zebrafish larvae, \*\*\*\* $P = 1.97E-7$ , Welch's  $t$ -test, two-sided).

responses were similar to those triggered by field stimulation (Fig. 4E, left). In line with previous reports<sup>32</sup>, cardiomyocytes under adrenergic activation exhibited significantly larger spontaneous Rhod-2 transients, concomitant with faster responses from NEMOer-f (Fig. 4E, right; Supplementary Fig. 6B, C). The observed phenomenon—larger cytoplasmic Ca<sup>2+</sup> transients despite similar relative changes in ER Ca<sup>2+</sup>—can be attributed to SR Ca<sup>2+</sup> overload induced by NE in cardiac muscle cells. Under SR overload conditions, the elevated basal SR Ca<sup>2+</sup> level results in a larger absolute Ca<sup>2+</sup> release for a given relative change.

We further assessed the ability of NEMOer-f to detect Ca<sup>2+</sup> blinks, the elementary decreases in SR Ca<sup>2+</sup> level leading to Ca<sup>2+</sup> sparks, the fundamental units of excitation-contraction coupling in cardiomyocytes. We successfully observed the Ca<sup>2+</sup> spark-blink pairs by Rhod-2 and NEMOer-f, respectively (Fig. 4F). Similar to previous reports<sup>22,30</sup>, the Rhod-2 signal peaks earlier than the SR Ca<sup>2+</sup> indicator. This phenomenon suggests that the cytosolic Ca<sup>2+</sup> spark reaches its peak when the decaying SR Ca<sup>2+</sup> release rate (due to decaying SR Ca<sup>2+</sup> concentration) is balanced by the increasing Ca<sup>2+</sup> diffusion rate (due to increasing local cytosolic Ca<sup>2+</sup> concentration). Afterward, the corresponding SR Ca<sup>2+</sup> blink reaches its nadir when SR Ca<sup>2+</sup> release terminates, outlasting the peak of a Ca<sup>2+</sup> spark. The peak amplitude of Ca<sup>2+</sup> blink indicated by NEMOer-f ( $\Delta F/F_0 = 0.17 \pm 0.01$ ), much larger than the Fluo-5N signal documented in rabbit muscle cells<sup>22,33</sup>. The duration of blink response indicated by NEMOer-f was slower than those reported by Fluo-5N. Further researches are needed to determine if the observed effect is due to the slower speed of NEMOer-f or facilitated Ca<sup>2+</sup> diffusion by Fluo-5N, a smaller Ca<sup>2+</sup> buffer molecule within SR. Nevertheless, to the best of our knowledge, this marks the first measurement of Ca<sup>2+</sup> blinks with genetically encoded Ca<sup>2+</sup> sensors, underscoring NEMOer-f's exceptional sensitivity.

#### In vivo performance of NEMOer indicator in zebrafish

The successful detection of Ca<sup>2+</sup> blinks with NEMOer-f in cardiac cells prompted us to test its performance in muscle cells in vivo. We took

advantage of larval zebrafish that is optically transparent for live imaging. We constructed Tol2 transposase-based transgenic vectors that express codon-optimized NEMOer-f specifically in the SR of muscle cells using the  $\beta$ -actin promoter<sup>34</sup>. By injecting the fertilized eggs at their 1-cell stages, we obtained larvae with transient expression of NEMOer-f and imaged sparsely labeled muscle cells on day 5 post fertilization (dpf) (Fig. 5A). As expected, the baseline fluorescence of NEMOer-f indicated the SR localization of the sensor in muscle cells with a typical striated morphology (Fig. 5B). We also performed parallel experiments using G-CEPIA1er following the same procedures. When muscles contracted, NEMOer-f fluorescence exhibited robust signals with a sharp decrease followed by a slow rising phase (Fig. 5C, D, Supplementary Video 4). G-CEPIA1er detected spontaneous Ca<sup>2+</sup> releases in fewer than 22% cells, with a median nadir amplitude of 0.15 (Supplementary Video 5). In contrast, NEMOer-f successfully reported these events in 48% cells, with responses 2.2 times larger (Fig. 5D, E). These data demonstrate that NEMOer-f functions in intact animals to detect spontaneous Ca<sup>2+</sup> releases in SR and is indeed a superior indicator to G-CEPIA1er.

Overall, here we reported NEMOer, a highly sensitive green GECIs for ER/SR with large dynamics. In comparison to commonly used GECIs derived from GCaMP-like series, such as G-CEPIA1er, NEMOer indicators show 10-fold higher brightness with the dynamic ranges 50 times larger, enabling the detection of physiological ER/SR Ca<sup>2+</sup> dynamics with significantly larger signals. NEMOer sensors also exhibit significantly enhanced photochemical properties, showing minimal sensitivity to physiological pH variations and enduring 50 times more illumination without apparent bleaching. These ideal properties make NEMOer compatible with super-resolution recording of SR/ER Ca<sup>2+</sup> homeostasis and dynamics. Remarkably, the fast NEMOer variant, NEMOer-f, stands out as the inaugural GECI that enables the detection of Ca<sup>2+</sup> blink, the elementary Ca<sup>2+</sup> releasing signal from SR of cardiomyocytes, as well as in vivo detection of spontaneous SR Ca<sup>2+</sup> releasing event in a model organism zebrafish. Collectively, the exceptionally

dynamic NEMOer sensors emerge as the premier choice for monitoring  $\text{Ca}^{2+}$  dynamics and homeostasis in mammalian cells, particularly within muscle cells.

## Methods

### Ethical statement

Animal experiments involving cultured primary neurons were approved by the Animal Care and Use Committee of the University of Science and Technology of China (Approval No. USTCA-CUC26120223022). Experiments involving cultured neonatal and adult rat cardiomyocytes were approved by the Institutional Animal Care and Use Committee of Peking University (Permit No. Isc-wangsq-1). All experimental procedures involving zebrafish were approved by the Institutional Animal Care and Use Committee of the Center for Excellence in Brain Science and Intelligence, Chinese Academy of Sciences (Approval No. NA-082-2024). We adhered to all relevant ethical guidelines and regulations.

### Plasmids construction and recombinant adenovirus production

ER-GCaMP6-150 and superfolder turquoise2<sup>ox</sup> (sfTq2<sup>ox</sup>)<sup>35</sup> were synthesized and incorporated into a pCDNA3.1(+) vector by BGI Geneland Scientific Co., Ltd, Jiangsu, China. Zebrafish codon-optimized NEMOer-f and G-CEPIA1er were synthesized by the entrusted company, Beijing Tsingke Biotech Co., Ltd., Beijing, China. The construction of other plasmids followed previously described methods. Briefly, target fragments were PCR amplified from corresponding templates, and the vector backbone was linearized with appropriate restriction enzymes. Corresponding mutations or substitutions were all included in primers. Fragments were then reassembled and inserted into the linearized vector utilizing a Ready-to-Use Seamless Cloning Kit (B632219, Sangon Biotech, Shanghai, China). Plasmids were all confirmed by sequencing. The vector backbones were linearized using the following restriction enzymes: BamHI and EcoRI for pCDNA3.1, EcoRI and XhoI for pTol2- $\beta$ -actin, and NcoI and XhoI for pET28a. The recombinant plasmids were amplified in the DH5 $\alpha$  strain (Vazyme Co., Ltd, Jiangsu, China).

To construct a variant library of NEMOer candidates, we performed PCR amplification of NEMOs<sup>23</sup>, incorporating known  $\text{Ca}^{2+}$ -affinity-reducing mutations<sup>26</sup> via primers. Subsequently, we added the endoplasmic reticulum localization signal sequence from GCEPIA1er<sup>26</sup> and the coding sequence for ER-resident sequence KDEL to the N and C-termini of the constructs, respectively. Then, we reassembled and inserted them into a pCDNA3.1 vector backbone. To construct the TurN (mTurquoise2-NEMO)/TuNer (mTurquoise2-NEMOer) plasmids, we amplified the coding sequence of sfTq2<sup>ox</sup>- $\Delta$ C11 from pCDNA3.1(+)-sfTq2<sup>ox</sup> and the coding sequences of NEMO/NEMOer- $\Delta$ N5 from NEMO/NEMOer, respectively. Subsequently, we reassembled and inserted them into a custom-made pCDNA3.1(+) vector with puromycin resistance. To generate the mKate-P2A-GECI plasmids, we assembled the coding sequence of mKate-P2A, which was amplified from the mKate-P2A-NEMO plasmid<sup>23</sup>, along with the coding sequences of NEMOer/GCEPIA1er, into the custom-made pCDNA3.1 vector. For expression in *Danio rerio*, codon-optimized NEMOer-f and G-CEPIA1er were subcloned into the pTol2- $\beta$ -actin vector, resulting in the generation of pTol2- $\beta$ -actin: NEMOer-f and pTol2- $\beta$ -actin: G-CEPIA1er.

The NEMOer-f gene sequences were amplified and inserted into pENTR2B vector (Invitrogen). The adenovirus was produced using the adenoviral expression system (Invitrogen) in HEK293A cells.

The sequences of primers used to generate GECI constructs are provided in Supplementary Table 7.

### Bacterial expression and protein purification

Transetta (DE3) bacteria (TransGen Biotech, Beijing, China) were transformed with pET28a plasmids carrying GECI coding sequences

and cultured in LB medium until reaching an optical density (OD) of 0.5. Protein expression was then induced overnight at 20 °C by adding 300 mM isopropyl- $\beta$ -D-thiogalactoside (IPTG). The recombinant proteins were purified following a previously described protocol<sup>36</sup>. Briefly, cells were harvested by centrifugation and re-suspended in 20 mL buffer 1 (mM, 20 Tris, 300 NaCl and 1 imidazole, pH 7.2). Cells were initially lysed and subsequently subjected to ultrasonic disruption, followed by incubation with 1 mL Ni Sepharose (17-5318-01, GE Healthcare, Piscataway, NJ, USA) to enrich recombinant GECI proteins with histidine-tags. The columns were sequentially washed with 20 mL buffer 1 and 10 mL buffer 2 (mM, 20 Tris, 500 NaCl, and 10 imidazole, pH 7.2). Finally, the GECI proteins were eluted using 5 mL buffer 3 (mM, 20 Tris, 100 NaCl, and 300 imidazole, pH 7.2).

### In vitro $\text{Ca}^{2+}$ titrations and kinetics measurements

The fluorescence intensity from buffer solutions containing 50  $\mu\text{g}/\text{mL}$  GECI proteins, used to calculate  $\text{Ca}^{2+}$  dissociation constant ( $K_d$ ), were recorded by a multi-mode microplate reader (Flexstation 3, Molecular Devices, USA). The buffer solution contained 130 mM KCl, 50 mM MOPS<sup>15</sup>, and  $\text{CaCl}_2$  with varying concentrations ranging from 0 mM to 128 mM (pH 7.2). The excitation/emission wavelengths of GCEPIA1er and NEMOer were 485 /510 nm and 490/520 nm with 10 nm bandpass, respectively.  $\text{Ca}^{2+}$  titration curves of  $\text{Ca}^{2+}$  concentration versus relative fluorescence intensity were then plotted and fit with specific binding with the hill slope function<sup>23</sup> in Prism 9.5 software.

The fluorescence traces used to calculate disassociation kinetics ( $k_{off}$ ) were recorded using a stopped-flow spectrometer (SX20, Applied Photophysics Ltd., United Kingdom) with a 2-mm path length and a 1.1 ms dead time at room temperature. Buffer A contained 50  $\mu\text{g}/\text{mL}$  GECI proteins, 1 mM  $\text{Ca}^{2+}$ , 50 mM MOPS, 100 mM KCl, pH 7.4<sup>14</sup>. Buffer B contained 10 mM EGTA, 50 mM MOPS, 100 mM KCl, pH 7.4. Subsequently, changes in fluorescence were monitored in response to rapidly mixing with buffers A and B. The fluorescence intensity changes of GECIs were recorded using a 515 nm long-pass filter with excitation at 488 nm. The  $k_{off}$  value was determined by fitting the fluorescence decay curve with a single exponential function using Prism 9.5 software.

### Spectra recording and measurement of quantum yields of GECIs

Purified proteins were diluted to a final concentration of 50-100  $\mu\text{g}/\text{mL}$  in a buffer containing 130 mM KCl, 50 mM MOPS, and supplement with or without 128 mM  $\text{CaCl}_2$ , pH 7.2. Fluorescence spectra were measured with a FS5 spectrophotometer (Edinburgh Instrument, Scotland) controlled by Fluoracle 2.15.2 software. Absorption spectra were measured with an ultraviolet and visible spectrophotometer (UV2600, Shimadzu, Japan) controlled by UVProbe 2.42 software.

The emission spectra and optical density(OD) used to calculate Quantum yields ( $\Phi$ ) of GECIs were determined with a FS5 spectrophotometer and an ultraviolet and visible spectrophotometer<sup>23</sup>. We used the obtained the emission spectra to calculate the total integrated fluorescence intensity with different concentrations of GECI protein. Linear regression of integrated fluorescence intensity and absorbance values to get the slopes (S).  $\Phi$  was determined by the equation:  $\Phi_{\text{protein}} = \Phi_{\text{standard}} \times (S_{\text{protein}}/S_{\text{standard}})$ <sup>9</sup>. The reference standards are fluorescein ( $\phi = 0.925$ ) and TOLLES ( $\phi = 0.79$ ) in 0.1 M NaOH<sup>37</sup>, excited at 470 nm and 405 nm, respectively<sup>38</sup>.

### Chromophore extinction coefficients

The absorption spectra of buffer solutions containing 200  $\mu\text{g}/\text{mL}$  GECI proteins, used to calculate extinction coefficients ( $\epsilon$ ), were recorded by Flexstation 3. Buffer solutions containing 30 mM trisodium citrate, 30 mM borate with varying pH values were supplemented with or without 128 mM  $\text{CaCl}_2$ . pKa values were then obtained with previously described calculations and curve-fittings performed by Prism

9.5 software employing specific-binding-with-Hill-slope function<sup>23</sup>. Error bars represent SEM.

### Cell isolation and cultures

**Culture of non-excitabile cell lines.** HEK293, HeLa and COS-7 cells (ATCC, cat#: CRL-1573, CL-0101 and CRL-1651, respectively) were grown at 37 °C in a humidified atmosphere containing 5% CO<sub>2</sub> in DMEM (HyClone, Chicago, IL, USA) with 10% fetal bovine serum (cat: FBSSA500-S, AusGeneX, Australia), 5% penicillin and streptomycin (Thermo Scientific, Waltham, MA, USA).

### Primary dissociated hippocampal and cortical neuronal cultures.

The cultured of primary hippocampal and cortical neurons involves a meticulous process starting with the dissection of hippocampi from both sides were dissected from embryonic day 18 CD<sup>®</sup>(SD) IGS rats of either gender using dissection tools previously sterilized by autoclaving. The dissected tissues are treated with a 0.25% trypsin solution (Sigma-Aldrich) at 37 °C for 15 min, followed by gentle shaking at 5-minute intervals to ensure thorough digestion. Subsequently, the dissected tissues were washed with Hanks' balanced salt solution (HBSS) without Ca<sup>2+</sup> and Mg<sup>2+</sup> (Thermo Fisher) to remove debris and blood, followed by pipetting with a Pasteur glass tube (15 mm) in DMEM-F12 (with L-glutamine +10% FBS) complete medium (Thermo Fisher) to obtain a cell suspension. The dissociated hippocampal and cortical neurons were plated on 50k cells/18 mm or 300k cells/25 mm coverslips in 12-well plates or 6-well plates, which were coated overnight with 0.01% poly-L-lysine (Sigma-Aldrich, Cat# P1274) at 37 °C. On the first day of culture, the neurons were incubated in DMEM-F12 (with L-glutamine +10% FBS) complete medium in a 5% CO<sub>2</sub> atmosphere at 37 °C to facilitate initial neuron adhesion and viability in the optimal developmental growth conditions. After 24 h of plating, half of the plating medium was replaced with fresh neurobasal medium without serum (with 2% B27, 0.5 mM L-glutaMAX, 37.5 mM NaCl) and once every 4 days thereafter. Neurons are prepared for experimental use following a development period of 18–20 days in culture.

### Neonatal and Adult rat cardiomyocytes isolation and culture.

Hearts were excised from 1-day rats and immersed in ice-cold Hanks solution (Sigma) supplemented with NaHCO<sub>3</sub> (3.6 mM) and taurine (30 mM). The cardiac tissue was subsequently minced into fragments and subjected to sequential enzymatic digestion with 5 mL pre-warmed collagenase II (Worthington, 0.08%) and trypsin solution (Yeasen, 0.1%) at 37 °C. After each 5–6 min digestion interval, the supernatant was collected and immediately neutralized with FBS. Cell suspensions were centrifuged at 800g for 5 min, followed by supernatant removal and resuspension in DMEM (Invitrogen) containing 10% FBS (Gibco) and 0.1 mM 5-bromo-2'-deoxyuridine (Sigma). Fresh enzymatic solution was applied to the remaining tissue fragments, with this digestion-neutralization cycle repeated 8–10 times until complete tissue dissociation. Myocytes were plated at 5 × 10<sup>5</sup> cells/3.5 cm dish.

Adult ventricular cardiomyocytes were enzymatically isolated as previously described<sup>39</sup>. Briefly, hearts were rapidly removed from anesthetized adult Sprague-Dawley rat and perfused using Ca<sup>2+</sup>-free Tyrode's solution (in mM: 120 NaCl, 4 KCl, 1.2 MgCl<sub>2</sub>, 1.5 NaH<sub>2</sub>PO<sub>4</sub>, 20 NaHCO<sub>3</sub>, 10 glucose, 30 taurine, 95% O<sub>2</sub>/5% CO<sub>2</sub> saturated) in a Langendorff system. Collagenase Type II (0.7 mg/mL) (Worthington Biochemical) was used to digestion of the heart into single cells. After digestion, the myocardium tissue was cut into small pieces and filtered into Ca<sup>2+</sup>-free Tyrode's solution with a sieve, then replaced with gradient Ca<sup>2+</sup> solution, resulting in a final solution with 1 mM Ca<sup>2+</sup>. Freshly isolated cardiomyocytes were plated on laminin-coated (Sigma) culture dishes for 20 min, and then the attached cells were maintained in M199 medium (Gibco) at 37 °C under 5% CO<sub>2</sub> until usage.

### Gene transfections

**Gene transfection animal cell lines.** Gene transfection of cells was completed with electroporation (Bio-Rad Gene Pulser Xcell system, Hercules, CA, USA). The electroporation protocol was a voltage step pulse (180 V, 25 ms) using 4 mm cuvettes and 0.4 mL OPTI-MEM medium. Transfected cells were seeded on round coverslips and cultured with DMEM. Imaging experiments were carried out 24 h after transfection.

### Transfection for primary dissociated hippocampal and cortical neurons.

Cultured neurons were transfected with 0.5–1 μg plasmids G-CEPIA1er or NEMOer -encoding plasmids at approximately 10–11 DIV using a calcium phosphate transfection kit (Takara, Cat# 631312). Specifically, cultured neurons on coverslips were transferred to a new 12-well plates or 6-well plates with pre-warmed DMEM-F12 (with L-glutamine + 25% 1 M HEPES) complete medium. Mix plasmids with 10% of 2 mM CaCl<sub>2</sub> in ddH<sub>2</sub>O. Subsequently, the DNA-containing mixed solution was transferred eight times into 2×HBS solution, vortexing for 3 s after each transfer. The mixture was then incubated for 15–20 min at room temperature and added dropwise to the culture 12-well plates or 6-well plates with medium. When an evenly distributed layer of precipitate particles was observed across the neurons (approximately 2 h later), the DNA-Ca<sup>2+</sup>-phosphate precipitates were dissolved using 1×HBS solution (pH 6.8). The transfected neurons were then transferred back to their original 12-well plates or 6-well plates containing neurobasal medium.

### Gene transfection of rat cardiomyocytes.

For adenovirus-mediated gene expression of adult cardiomyocytes. Cells were infected with adenoviruses carrying the NEMOer-f calcium sensor at a multiplicity of infection (m.o.i.) of 30. Confocal imaging was performed 48 h after virus infection. As to neonatal rat cardiomyocytes, 36 to 48 hr after cell culture, 4 μg plasmids was transiently transfected into cells with Lipofectamine 3000 according to the manufacturer's instructions.

### Fluorescence imaging

The fluorescence imaging was performed using a ZEISS observer Z1 imaging system controlled by Slidebook 6.0.23 software (Intelligent Imaging Innovations, Inc.)<sup>23</sup>. Cells grown on coverslips were immersed in a physiological salt solution (107 mM NaCl, 7.2 mM KCl, 1.2 mM MgCl<sub>2</sub>, 11.5 mM glucose, 20 mM HEPES-NaOH at pH 7.2), supplemented with 0.1% BSA. The excitation/emission filters used: NEMOer (500 ± 12/542 ± 13 nm), G-CEPIA1er/ER-GCaMP6-150 (470 ± 11 /510 ± 14 nm) and TurN/TuNer (For YFP channel, 500 ± 10/ 535 ± 15 nm; for CFP channel, 438 ± 12 /470 ± 12 nm). Fluorescence was collected every two seconds, and the mean fluorescent intensity of the corresponding regions was exported for analysis using Matlab 2023b (The MathWorks, Natick, MA, USA), and the results were plotted using Prism 9.5 software. The perfusion rate is 6.7 s/mL, allowing the complete exchange of the solution in the perfusion chamber within 1.5 s. Error bars denote SEM.

### Confocal imaging

**Confocal imaging of COS-7 cells.** Recordings were undertaken with a ZEISS LSM880 microscope equipped with 63x oil objective (NA 1.4) and ZEN 2.1 software. For measurement of TuNer-m fluorescence ratio excited by optimal excitation with and without calcium, excitation was set at 458 and 514 nm, with the emission collected at 460–500 nm and 520–600 nm. The acquired images were analyzed using Image J and Matlab 2023b software. To improve image resolution and contrast, the software MicroscopeX FINER(Computational Super-resolution Biotech Co.,Ltd, Guangzhou, China), which uses sparse deconvolution, was utilized, following the methodology reported previously<sup>27</sup>. To estimate ER Ca<sup>2+</sup> level based on the ratiometric measurement using TuNer-m (Supplementary Fig. 4C–E), ER Ca<sup>2+</sup> level was calculated using the

following equation:  $[Ca^{2+}]_{free} = \frac{R - R_{min}}{R_{max} - R_{min}} \times K_d$ , where  $R = F_{NEMOer-m} / F_{sTq2ox}$ ,  $n = 1.28$  and  $K_d = 958.67 \mu\text{M}$ .

**Confocal line-scan imaging of cardiomyocytes.** The imaging was performed on a confocal microscope (LSM-710; Carl Zeis) equipped with an argon laser (488 nm) and 40 $\times$ , 1.0 N.A. water immersion objective. Myocytes were loaded with 10  $\mu\text{M}$  Rhod2-AM (Invitrogen) under 37  $^{\circ}\text{C}$  for 10 min ( $Ca^{2+}$  transient and SR load measurement) or 20  $\mu\text{M}$  Rhod2-AM (Invitrogen) under 37  $^{\circ}\text{C}$  for 5 min ( $Ca^{2+}$  spark measurement), and the experiments were performed within 1 hr after loading. In pacing  $Ca^{2+}$  transient recording experiments, 15 V, 1 Hz field stimulation to the myocytes. For  $Ca^{2+}$  transient,  $Ca^{2+}$  spark, and SR load measurement, line-scan images were acquired at sampling rates of 3.78 ms/line, the excitation was at 488 and 543 nm, and their fluorescence emission were collected at 490 to 550 and 560 nm to 800 nm. The fluorescence-time curves of image were analyzed by python, the  $\Delta F/F_0$  ( $(F - F_0)/F_0$ ), time to peak (the time of  $F_{max}$ ) and  $\tau_{90}$  (decay time of 90% fluorescence change of  $F_{max}$ ) were calculated from curve by matlab R2018a program.

**$Ca^{2+}$  imaging and quantitative analysis of fluorescence intensity in neurons.** Cultured hippocampal neurons of DIV 18–20 were imaged using a W1 spinning disc confocal microscope (Ti2-E, NIKON) with a 100  $\times$  oil-immersion objective (1.45 NA, NIKON) in extracellular solution (120 mM NaCl, 3 mM KCl, 10 mM glucose, 10 mM HEPES-NaOH, 2 mM  $MgCl_2$ , and 2 mM  $CaCl_2$ , pH 7.4). Field stimulations were performed in a stimulation chamber (Warner Instruments, RC-49MFSH) with a programmable stimulator (Master-8, AMPI). The hippocampal neurons were imaged with an exposure time of 200 ms with consecutive and uninterrupted acquisition. For pharmacological experiments, 50  $\mu\text{M}$  CPA (MCE, Cat# HY-N6771) was incubated for 1 h in neurobasal medium at 37  $^{\circ}\text{C}$ . In the control group, neurons were incubated with DMSO (dimethyl sulfoxide, Sigma) for the corresponding time.

Cultured cortical neurons of DIV 16–18 were imaged with a ZEISS LSM880 microscope equipped with 63 $\times$  oil objective (NA 1.4) and ZEN 2.1 software in extracellular solution (124 mM NaCl, 3 mM KCl, 2 mM  $CaCl_2$ , 2 mM  $MgCl_2$ , 10 mM HEPES, 10 mM D-Glucose, pH 7.4).  $Ca^{2+}$  release from cultured cortical neuronal ER was induced by 100  $\mu\text{M}$  DHPG (MCE, Cat# HY-12598A). The cortical neurons were imaged with an exposure time of 2.2 s with consecutive and uninterrupted acquisition.

All the quantifications of fluorescent signals in neuronal cultures were performed on the secondary dendrites and somata of transfected neurons. A region of interest (ROI) was chosen based on the imaging criteria, e.g., the quality of fluorescent signals, the background level. ROI of dendrites, somata, and spines were manually defined in ImageJ for the calculation of mean fluorescent signal  $F_s$ . A similar region near the dendrites and somata of interest was selected for the calculation of fluorescent background  $F_b$ . The effective signal was calculated as  $F = F_s - F_b$ . Since all our quantifications were based on  $F$  normalized with the averaged fluorescence intensity within the region during the baseline period, the area of defined polygon would have no impact on the normalized  $F$ . We also simultaneously monitor x-y drift to ensure that the identification of the target area in ImageJ does not deviate from the defined ROI.

### Multimodality Structured Illumination Microscopy (Multi-SIM) imaging

SIM images were acquired on a Multi-SIM imaging system<sup>40</sup> (NanoInsights-Tech Co., Ltd.) equipped with a 100  $\times$  1.49 NA oil objective (Nikon CFI SR HP Apo), and a Photometrics Kinetix camera. SIM images were collected with VSIM 2.2.1.10 software. The SIM images of COS-7 cells expressing TuNer-m were taken using low NA GI-SIM mode with

laser power set to 300 mW (445 nm) and an exposure time of 30 ms, enabling authentic simultaneous detection in the 415–475 nm and 500–550 nm range using two detectors. Bleed-through correction was performed to ensure accurate spectral separation. Images were then reconstructed using the SIM Imaging Analyzer software (NanoInsights-Tech). During the acquisition of images, cells were in a humidified chamber maintained at 37  $^{\circ}\text{C}$  in the presence of 5%  $CO_2$ . The reconstructed images were analyzed using Image J software.

### Animals

CD<sup>0</sup>(SD) IGS rats were obtained from Charles River and used for the culture of primary hippocampal and cortical neurons. The rats were group-housed in cages of three under a 12-hour light/dark cycle (lights on at 7 a.m.) in a stable environment (temperature maintained between 22  $^{\circ}\text{C}$  and 24  $^{\circ}\text{C}$ ), with water and food available ad libitum. Female CD<sup>0</sup>(SD) IGS rats were sacrificed at 18 days of gestation for neuron culture. For cardiomyocyte isolation and culture, adult male SD rats aged 8–12 weeks were used, and neonatal ventricular myocytes were isolated from 1-day-old SD rats. Adult and larval zebrafish (*Danio rerio*) of the *nacre* background were maintained at 28.5  $^{\circ}\text{C}$  under a 14-hour/10-hour light/dark cycle. Adult zebrafish were fed twice daily. Zebrafish larvae at 5–6 dpf were used for imaging.

### Experiment in zebrafish (*Danio rerio*)

To generate transient expression larvae for imaging, mating pairs of adult fish of *nacre* background were set up to avoid dark pigmentation. Injection mix contained 25 ng/ $\mu\text{L}$  of pTol2- $\beta$ -actin: NEMOer-f or pTol2- $\beta$ -actin: G-CEPIA1er and 25 ng/ $\mu\text{L}$  of Tol2 mRNA. Approximately 1 nL of the cocktail was injected into fertilized eggs. Adult and larval zebrafish were maintained at 28 degrees on a 14 h/10 h light/dark cycle. All experiments were conducted in 10% Hank's solution containing (in mM): 140 NaCl, 5.4 KCl, 0.25  $Na_2HPO_4$ , 0.44  $KH_2PO_4$ , 1.3  $CaCl_2$ , 1.0  $MgSO_4$ , and 4.2  $NaHCO_3$  (pH 7.2). All experimental procedures were approved by Center for Excellence in Brain Science and Intelligence, Chinese Academy of Sciences.

Confocal microscopy was performed using Olympus FV3000 upright microscope with a LUMPlanFL N 40 $\times$  water immersion objective (N.A. 0.8, W.D. 3.3). Scanning speed was 1 Hz and a single plane was imaged for time-lapse imaging. The frame size was set as 512  $\times$  512 at 16-bit depth, and the actual scan size was slightly cropped to allow 1 Hz speed. The 5 dpf or 6 dpf zebrafish larvae were embedded sideways in 2% low-melting agarose (Invitrogen, 16520100) under system water. Zebrafish larvae were neither anesthetized nor paralyzed. Time-lapse images were registered using StackReg to correct mild drifts and fluorescence values of ROI were measured in Fiji. Baseline fluorescence ( $F_0$ ) was defined as the top fifteen percentile value and normalized fluorescence changes ( $\Delta F/F_0$ ) were calculated in MATLAB R2020b.

### Statistics and reproducibility

Sample sizes were determined based on well-established studies in the field and the observed animal-to-animal variability during the experiments. For the detection of the performance of transiently expressed NEMOer variants in non-excitabile cells (HEK293 cells, HeLa cells, and COS7 cells), the sample size involved at least 3 experimental repeats, with 5 to 20 cells per repeat. For detecting the performance of transiently expressed NEMOer variants in cardiomyocytes, 3 to 32 cells from 3 adult rats and 60 neonatal rats were used, with at least 3 experimental repeats. For detecting the responses of NEMOer variants in dissociated rat hippocampal neurons excited by electric field stimulation, the sample size involved at least 10 neurons from three different primary hippocampal neuron cultures. The sample size for detecting the responses of NEMOer variants in dissociated rat cortical neurons involved at least 7 neurons from 30 fetal rats, with 3 experimental repeats. For detecting the performance of transiently expressed NEMOer-f and G-CEPIA1er sensors in zebrafish, 4 zebrafish larvae

per sensor were used. The specific replicates for each experiment are provided in the corresponding figure legends.

No data were excluded from the analyses. Multiple experiments using zebrafish or cells were conducted to assess the reproducibility of our findings. At least three independent repeats were performed for each set of experiments, and all attempts at replication were successful, confirming the reliability of our results.

Samples were allocated randomly, and investigators were blinded to group allocation during data collection and analysis.

### Reporting summary

Further information on research design is available in the Nature Portfolio Reporting Summary linked to this article.

### Data availability

All relevant data from this study, including generated and analyzed datasets, are provided in the published article and its supplementary information files. The relevant data generated in this study are provided in the Source Data file. Source Data file is provided with this paper. Source data are provided with this paper.

### Code availability

The Matlab code used in this study consists of simple scripts for basic matrix operations and is available at Zenodo (<https://doi.org/10.5281/zenodo.15094049>).

### References

- Clapham, D. E. Calcium signaling. *Cell* **131**, 1047–1058 (2007).
- Berridge, M. J. The endoplasmic reticulum: a multifunctional signaling organelle. *Cell Calcium* **32**, 235–249 (2002).
- Schwarz, D. S. & Blower, M. D. The endoplasmic reticulum: structure, function and response to cellular signaling. *Cell Mol. Life Sci.* **73**, 79–94 (2016).
- Zheng, S., Wang, X., Zhao, D., Liu, H. & Hu, Y. Calcium homeostasis and cancer: insights from endoplasmic reticulum-centered organelle communications. *Trends Cell Biol.* **33**, 312–323 (2023).
- Parkkinen, I. et al. Pharmacological regulation of endoplasmic reticulum structure and calcium dynamics: importance for neurodegenerative diseases. *Pharm. Rev.* **75**, 959–978 (2023).
- Miyawaki, A. et al. Fluorescent indicators for Ca<sup>2+</sup> based on green fluorescent proteins and calmodulin. *Nature* **388**, 882–887 (1997).
- Tallini, Y. N. et al. Imaging cellular signals in the heart in vivo: Cardiac expression of the high-signal Ca<sup>2+</sup> indicator GCaMP2. *Proc. Natl Acad. Sci. USA* **103**, 4753–4758 (2006).
- Chen, T. W. et al. Ultrasensitive fluorescent proteins for imaging neuronal activity. *Nature* **499**, 295–300 (2013).
- Zhao, Y. et al. An expanded palette of genetically encoded Ca<sup>2+</sup> indicators. *Science* **333**, 1888–1891 (2011).
- Llinás, R., Blinks, J. R. & Nicholson, C. Calcium transient in pre-synaptic terminal of squid giant synapse: detection with Aequorin. *Science* **176**, 1127–1129 (1972).
- Tang, S. et al. Design and application of a class of sensors to monitor Ca<sup>2+</sup> dynamics in high Ca<sup>2+</sup> concentration cellular compartments. *Proc. Natl Acad. Sci. USA* **108**, 16265–16270 (2011).
- Deng, X. et al. Tuning protein dynamics to sense rapid endoplasmic-reticulum calcium dynamics. *Angew. Chem. Int. Ed.* **60**, 23289–23298 (2021).
- Reddish, F. N. et al. Rapid subcellular calcium responses and dynamics by calcium sensor G-Catcher+. *iScience* <https://doi.org/10.1016/j.isci.2021.102129> (2021).
- Henderson, M. J. et al. A low affinity GCaMP3 Variant (GCaMPer) for imaging the endoplasmic reticulum calcium store. *PLoS One* **10**, e0139273 (2015).
- Suzuki, J. et al. Imaging intraorganellar Ca<sup>2+</sup> at subcellular resolution using CEPIA. *Nat. Commun.* **5**, 4153 (2014).
- Li, J. et al. Visible light excited ratiometric-GEICs for long-term intracellular monitoring of calcium signals. *Cell Calcium* **87**, 102165 (2020).
- Luo, C., Wang, H., Liu, Q., He, W. & Xu, P. A genetically encoded ratiometric calcium sensor enables quantitative measurement of the local calcium microdomain in the endoplasmic reticulum. *Biophys. Rep.* **5**, 31–42 (2019).
- Farhana, I., Hossain, M. N., Suzuki, K., Matsuda, T. & Nagai, T. Genetically encoded fluorescence/bioluminescence bimodal indicators for Ca<sup>2+</sup> Imaging. *ACS Sens.* <https://doi.org/10.1021/acssensors.9b00531> (2019).
- Navas-Navarro, P. et al. GFP-Aequorin protein sensor for ex vivo and in vivo imaging of Ca<sup>2+</sup> dynamics in high-Ca<sup>2+</sup> organelles. *Cell Chem. Biol.* **23**, 738–745 (2016).
- Suzuki, J., Kanemaru, K. & Iino, M. Genetically encoded fluorescent indicators for organellar calcium imaging. *Biophys. J.* **111**, 1119–1131 (2016).
- Reddish, F. N., Miller, C. L., Gorkhali, R. & Yang, J. J. Calcium dynamics mediated by the endoplasmic/sarcoplasmic reticulum and related diseases. *Int. J. Mol. Sci.* **18**, <https://doi.org/10.3390/ijms18051024> (2017).
- Brochet, D. X. et al. Ca<sup>2+</sup> blinks: rapid nanoscopic store calcium signaling. *Proc. Natl Acad. Sci. USA* **102**, 3099–3104 (2005).
- Li, J. et al. Engineering of NEMO as calcium indicators with large dynamics and high sensitivity. *Nat. Methods* **20**, 918–924 (2023).
- de Juan-Sanz, J. et al. Axonal endoplasmic reticulum Ca<sup>2+</sup> content controls release probability in CNS nerve terminals. *Neuron* **93**, 867–881 e866 (2017).
- Wu, J. et al. Improved orange and red Ca<sup>2+</sup> indicators and photophysical considerations for optogenetic applications. *ACS Chem. Neurosci.* **4**, 963–972 (2013).
- Subach, O. M. et al. Novel genetically encoded bright positive calcium indicator NCaMP7 based on the mneongreen fluorescent protein. *Int. J. Mol. Sci.* **21**, <https://doi.org/10.3390/ijms21051644> (2020).
- Zhao, W. et al. Sparse deconvolution improves the resolution of live-cell super-resolution fluorescence microscopy. *Nat. Biotechnol.* **40**, 606–617 (2022).
- Bading, H. Nuclear calcium signalling in the regulation of brain function. *Nat. Rev. Neurosci.* **14**, 593–608 (2013).
- Deng, X. et al. Tuning protein dynamics to sense rapid endoplasmic-reticulum calcium dynamics. *Angew. Chem. Int. Ed. Engl.* **60**, 23289–23298 (2021).
- Lu, F. et al. Imaging sarcoplasmic reticulum Ca<sup>2+</sup> signaling in intact cardiac myocytes. *Circulation* **42**, 1503–1505 (2020).
- Bovo, E., Martin, J. L., Tyryfter, J., de Tombe, P. P. & Zima, A. V. R-CEPIA1er as a new tool to directly measure sarcoplasmic reticulum [Ca] in ventricular myocytes. *Am. J. Physiol. Heart Circ. Physiol.* **311**, H268–275 (2016).
- Shannon, T. R., Guo, T. & Bers, D. M. Ca<sup>2+</sup> scraps: local depletions of free [Ca<sup>2+</sup>] in cardiac sarcoplasmic reticulum during contractions leave substantial Ca<sup>2+</sup> reserve. *Circ. Res.* **93**, 40–45 (2003).
- Brochet, D. X., Xie, W., Yang, D., Cheng, H. & Lederer, W. J. Quark calcium release in the heart. *Circ. Res.* **108**, 210–218 (2011).
- Tao, R. et al. A genetically encoded ratiometric indicator for tryptophan. *Cell Discov.* **9**, 106 (2023).
- Meiresonne, N. Y. et al. Superfolder mTurquoise2ox optimized for the bacterial periplasm allows high efficiency in vivo FRET of cell division antibiotic targets. *Mol. Microbiol.* **111**, 1025–1038 (2019).
- Dana, H. et al. High-performance calcium sensors for imaging activity in neuronal populations and microcompartments. *Nat. Methods* **16**, 649–657 (2019).
- Wilkinson, J. G. Principles of fluorescence spectroscopy - Lakowicz. *Jr. Chem. Brit* **20**, 442–442 (1984).

38. Katayama, H. et al. Visualizing and modulating mitophagy for therapeutic studies of neurodegeneration. *Cell* **181**, 1176–1187.e16 (2020).
39. Yang, L. et al. Transcriptional regulation of intermolecular Ca(2+) signaling in hibernating ground squirrel cardiomyocytes: The myocardin-junctophilin axis. *Proc. Natl Acad. Sci. USA* **118**, <https://doi.org/10.1073/pnas.2025333118> (2021).
40. Guo, Y. et al. Visualizing intracellular organelle and cytoskeletal interactions at nanoscale resolution on millisecond timescales. *Cell* **175**, 1430–1442.e1417 (2018).
41. Wu, S., Skolnick, J. & Zhang, Y. Ab initio modeling of small proteins by iterative TASSER simulations. *BMC Biol.* **5**, 17 (2007).

## Acknowledgements

This work was supported by the National Natural Science Foundation of China (92254301 and W2411015 to Y. W., 32171026 to Y. M., 32250003 and 32230048 to S.-Q.W.), STI2030-Major Projects (2021ZD0202503 to A.-H. T., 2021ZD0204500 and 2021ZD0203704 to Y. M.), the National Key Research and Development Program of China (2020YFA0112200 to A.-H. T. and 2024YFA0916804 to S.-Q.W.), China Postdoctoral Science Foundation General Program (2022M723246 to Z. W.), the Natural Science Foundation of Anhui Province (2408085QH256 to J.-H.C.), Scientific Instrument Developing Project of the Chinese Academy of Sciences (YJKYYQ20210029 to Y. M.) and the Ministry of Science and Technology of China (2019YFA0802104 to Y. W.). We would like to thank the Experimental Technology Center for Lifesciences, Beijing Normal University and the National Center for Protein Sciences at Peking University. We thank Dr. Qian Hu and the Optical Imaging Facility from the Institute of Neuroscience for their support. We thank the Core Facility for Biomolecule Preparation and Characterization, Tsinghua University.

## Author contributions

Y. W., A.-H. T., S.-Q. W., and Y. M. supervised and coordinated the study. W. G. and J. L. designed and generated all the plasmid constructs, with help from Z.Z., J. L., W. G., and H. Z. performed the in vitro assays. W. G. performed all fluorescence imaging in non-excitabile cells, with help from J. L. and J. Z.. J. C. isolated and cultured primary cortical neurons with help from W. G. and P. L. J. C. performed confocal imaging of dissociated hippocampal neurons. W. G. performed confocal imaging of dissociated cortical neurons. Y. Z. performed confocal imaging of dissociated cardiac cells, and Z. X. analyzed spark and blink data. W. G., A. J., and H. Z. performed Multi-SIM imaging on COS-7 cells under the guidance of Y. W. and D. L. Z. W. performed in vivo Ca<sup>2+</sup> imaging of zebrafish muscle cells with help from S. W. C. X. provided tech support

for live cell imaging. W. G., J. C., Y. Z., Z. W., J. L., and H. Z. analyzed data with input from the other authors. D. L. G., S. W., Y. M., T. H., and J. L. provided intellectual input to the manuscript. Y. M., A.-H. T. and Y. W. wrote the manuscript with inputs from all the other authors.

## Competing interests

The authors declare no competing interests.

## Additional information

**Supplementary information** The online version contains supplementary material available at <https://doi.org/10.1038/s41467-025-58705-6>.

**Correspondence** and requests for materials should be addressed to Yu Mu, Shi-Qiang Wang, Ai-Hui Tang or Youjun Wang.

**Peer review information** *Nature Communications* thanks Yi Shen, and the other, anonymous, reviewer(s) for their contribution to the peer review of this work. A peer review file is available.

**Reprints and permissions information** is available at <http://www.nature.com/reprints>

**Publisher's note** Springer Nature remains neutral with regard to jurisdictional claims in published maps and institutional affiliations.

**Open Access** This article is licensed under a Creative Commons Attribution-NonCommercial-NoDerivatives 4.0 International License, which permits any non-commercial use, sharing, distribution and reproduction in any medium or format, as long as you give appropriate credit to the original author(s) and the source, provide a link to the Creative Commons licence, and indicate if you modified the licensed material. You do not have permission under this licence to share adapted material derived from this article or parts of it. The images or other third party material in this article are included in the article's Creative Commons licence, unless indicated otherwise in a credit line to the material. If material is not included in the article's Creative Commons licence and your intended use is not permitted by statutory regulation or exceeds the permitted use, you will need to obtain permission directly from the copyright holder. To view a copy of this licence, visit <http://creativecommons.org/licenses/by-nc-nd/4.0/>.

© The Author(s) 2025